This is a preprint, the final version is subject to change, of the American Mineralogist (MSA)
Cite as Authors (Year) Title. American Mineralogist, in press.
(DOI will not work until issue is live.) DOI: http://dx.doi.org/10.2138/am.2014.4670

REVISION 1

Color of Mn-bearing gahnite: A first example of electronic transitions in heterovalent exchange coupled $^{IV}Mn^{2+}$-$^{VI}Mn^{3+}$ pairs in minerals

ULF HÅLENIUS[1]* AND FERDINANDO BOSI[2]

[1]Department of Geosciences, Swedish Museum of Natural History, Box 50007, SE-10405 Stockholm, Sweden

[2]Dipartimento di Scienze della Terra, Sapienza Università di Roma, Piazzale Aldo Moro, 5, I-00185 Rome, Italy

ABSTRACT

A natural yellow and transparent crystal of Mn-bearing, Mg-rich gahnite ($ZnAl_2O_4$) from Nordmark (Sweden) was studied by electron microprobe, single crystal X-ray diffraction and optical absorption spectroscopy. The empirical structural formula of the crystal, $^{T}(Zn_{0.52}Mg_{0.34}Mn^{2+}_{0.08}Al_{0.06})_{\Sigma 1.00}\,^{M}(Al_{1.88}Mn^{3+}_{0.06}Fe^{3+}_{0.01}Mg_{0.04}Mn^{2+}_{0.01})_{\Sigma 2.00}\,O_4$, shows that Mn^{2+} and Mn^{3+} are almost completely ordered at the T and M sites, respectively. The electronic absorption spectrum of the spinel shows, in addition to a strong UV-absorption edge (O^{2-}-Mn^{3+} and O^{2-}-Fe^{3+} ligand-metal charge transfers) and two broad $^{VI}Mn^{3+}$-bands, a set of relatively narrow absorption bands at energies comparable to those caused by spin-forbidden electron transitions in tetrahedrally coordinated Mn^{2+} in oxide spinel. However, the set of bands in the present spectrum is shifted to lower energies and they are intensified by approximately an order of magnitude compare to those recorded for spin-forbidden $^{IV}Mn^{2+}$-bands in spinel. These characteristic differences in combination with the determined cation distribution in the present gahnite demonstrates that electronic transitions in exchange coupled $^{IV}Mn^{2+}$-$^{VI}Mn^{3+}$ pairs cause its color.

Key words: Gahnite, crystal structure, electronic spectra

INTRODUCTION

Color is one of the fundamental physical properties that commonly is used for mineral identification. Color in minerals has also an economic dimension. The value of gems and also of several industrial minerals is strongly dependent on their colors. Consequently, knowledge about the processes that create mineral colors is important. The majority of the common ferromagnesian rock-forming minerals owe their characteristic colors and pleochroism to electronic transitions in iron cations that are present in their structures. These electronic processes occur at energies corresponding to those of visible light and they may either be electron excitations that take place between energy levels within single ions of Fe^{2+} or Fe^{3+} or more importantly, they may represent electron hopping between heterovalent neighboring cations in the crystal, the so called Fe^{2+}-Fe^{3+} intervalence charge transfer processes (IVCT).

Numerous examples of Fe-related IVCT processes as the main cause for color and pleochroism in the common silicates of the amphibole, pyroxene and mica mineral groups have been observed (Burns 1993 and references therein). Color caused by electron transitions in magnetically exchange coupled homonuclear cation pairs (ECP), trimers or larger clusters have also been documented in minerals (e.g., Rossman 1975; Rossman1976). Intensity enhanced absorption bands caused by exchange coupled heterovalent Fe^{2+}-Fe^{3+} pairs have been reported in spectra of tourmaline (Mattson and Rossman 1986) and spinel minerals (Taran et al. 2005). However, there exist a limited number of documented examples of non-iron IVCT or ECP processes that create color in minerals. Examples of heteronuclear

[1] E-mail: ulf.halenius@nrm.se

processes involving Fe are though known. The most common ones are Fe^{2+}-Ti^{4+} IVCT processes in silicates and oxide minerals (e.g., Mattson and Rossman 1988; Taran and Koch-Müller 2011).

In view of the large number of examples of Fe-related IVCT and ECP coloring processes in minerals it is surprising that the number of reported IVCT and ECP cases in Mn-bearing minerals are so scarce. Considering the terrestrial abundance of manganese, the natural occurrence of differently charged Mn-cations, cation radii that proxy those of iron cations, and the number of common Mn-bearing minerals, one would expect a comparable number of documented examples of Mn^{2+}-Mn^{3+} or Mn^{2+}-Me^{n+} IVCT or ECP causing mineral coloration. Rossman and Mattson (1986) suggested that Mn^{2+}-Ti^{4+} IVCT occurred in Mn-rich yellow tourmaline. In addition, exchange coupled pairs of octahedrally coordinated Mn^{2+} and tetrahedrally coordinated Fe^{3+} in trioctahedral micas have been proposed as the cause for the color and the reverse pleochroism in some phlogopite samples (Smith et al. 1982). Furthermore, Mn-related ECP processes have been proposed for a small number of minerals: Mn-bearing diopside (Hålenius and Skogby 1996), genthelvite-helvite solid solution minerals (Hålenius 2011), tephroite and rhodochrosite (Hålenius et al. 2007).

It is notable that in contrast to the above very restricted number of mineral examples, the coloring power of electronic transitions in exchange coupled pairs of Mn cations has long been known and documented for a large number of inorganic compounds (e.g., Ferguson et al. 1965b and 1966b; Lohr and McClure 1968). These cases demonstrate that Mn-related ECP-transitions may occur even in compounds diluted in manganese and also that ECP-transitions in homonuclear as well as heteronuclear Mn-related pairs are common (e.g., Ferguson et al. 1965a). Ferguson et al. (1966b) summarized theoretical considerations on the nature of the

ECP-transitions and the character of the selection rule relaxations that allow enhanced transition probabilities. Reviews on optical absorption spectroscopy of exchange coupled cation pairs, providing several examples of spectroscopic active homonuclear and heteronuclear 3*d* transition element pairs in chemical compounds, have been published by, e.g., Lohr (1972) and McCarthy (1988). Articles within different fields of physics and chemistry demonstrate the broad and continued interest in exchange interactions in transition metal pairs. Published studies on Ni^{2+}-Mn^{2+}(Ferguson et al. 1966a), Cu^{2+}-Mn^{2+} (Ferre and Regis 1978; Cador et al. 2000), Mn^{2+}-Mn^{3+} (Franz et al. 2003; Cox et al. 2011; Xie et al. 2012), Mn^{3+}-Mn^{3+} (Pelletier 1995) and Mn^{3+}-Mn^{4+} pairs (Birkelbach et al. 1998) are some examples that reflect this interest.

With the aim to explore the potential occurrence of electronic transitions in exchange coupled pairs of Mn in spinel minerals, we have studied a natural Mg-rich gahnite ($ZnAl_2O_4$) that contains an appreciable Mn-content by means of electron microprobe, single-crystal X-ray diffraction and single-crystal optical absorption technique.

EXPERIMENTAL

Sample

The studied gahnite single crystal was selected from a calcite-rich layer with hausmannite, manganosite and feitknechtite at the manganese ore at Kittelgruvan, Nordmark, Värmland, Sweden. The small (up 0.5 mm) gahnite single crystals occur as transparent, octahedra displaying a yellow color similar to those observed in synthetic Mn-bearing spinels (Bosi et al. 2007; Hålenius et al. 2011). The same selected crystal was used in all the performed experiments.

Single-crystal structure refinement

X-ray diffraction measurements were performed at Earth Sciences Department, Sapienza University of Rome, with a Bruker KAPPA APEX-II single-crystal diffractometer, equipped with CCD area detector (6.2 × 6.2 cm^2 active detection area, 512 × 512 pixels) and a graphite crystal monochromator, using MoKα radiation from a fine-focus sealed X-ray tube. The sample-to-detector distance was 4 cm. A total of 4268 exposures (step = 0.2°, time/step = 10 s) covering a full reciprocal sphere were collected. The orientation of the crystal lattice was determined from more than 500 strong reflections ($I > 100\ \sigma_I$) evenly distributed in the reciprocal space, and used for subsequent integration of all recorded intensities. Final unit-cell parameters were refined by means of the Bruker AXS SAINT program from ca. 1328 recorded reflections with $I > 10\ \sigma_I$ in the range $9° < 2\theta < 90°$. The intensity data were processed and corrected for Lorentz, polarization and background effects with APEX2 software program of Bruker AXS. The data were corrected for absorption using multi-scan method (SADABS). The absorption correction led to a significant improvement in R_{int}. No violation of $Fd\bar{3}m$ symmetry was noted. Sporadic appearance of forbidden space-group reflections was recognized as double reflections.

Structural refinements were carried out with the SHELXL program (Sheldrick 2008). Setting the origin at $\bar{3}m$, initial atomic positions for oxygen atoms were taken from the structure of spinel (Bosi et al. 2010). Variable parameters were overall scale factor, extinction coefficient, atomic coordinates, site scattering values expressed as mean atomic number (m.a.n.), and atomic displacement factors. No chemical constraint was applied during the refinement. To obtain the best values of statistical indexes ($R1$ and $wR2$) the oxygen site was modeled with neutral *versus* fully ionized oxygen scattering curves, while neutral curves were used for the cation sites. In detail, the T site was modeled considering the presence of Zn and Mg scattering factors, whereas the M site was modeled by Al scattering factor. Three full-matrix

refinement cycles with isotropic displacement parameters for all atoms were followed by anisotropic cycles until convergence was attained, that is, when the shifts in all refined parameters were less than their estimated standard deviation. No correlation over 0.7 between parameters was observed at the end of refinement. Table 1 summarizes structural parameters and refinement details.

Chemical analyses

Electron microprobe analyses were done by wavelength-dispersive spectroscopy with a Cameca SX50 instrument at the "Istituto di Geologia Ambientale e Geoingegneria (Rome, Italy), CNR", operating at an accelerating potential of 15 kV, a sample current of 15 nA and a spot size of 1 μm. Minerals and synthetic compounds were used as standards: magnetite (Fe), rutile (Ti), corundum (Al), periclase (Mg), sphalerite (Zn) and metallic Mn. The PAP matrix correction procedure (Pouchou and Pichoir 1991) was applied to reduce the raw data. The results are summarized in Table 2. Titanium was below its detection limits (0.03 wt%).

Optical absorption spectroscopy

Unpolarised, room-temperature optical absorption spectra in the spectral range 270-1100 nm (37 037-9091 cm^{-1}) were recorded on a 46 μm thick double-sided polished section of the single crystal at a spectral resolution of 1 nm using a AVASPEC-ULS2048X16 spectrometer attached via a 400 μm UV fiber cable to a Zeiss Axiotron UV-microscope. A 75 W Xenon arc was used as a light source and Zeiss Ultrafluar 10× lenses served as objective and condenser. The size of the circular measure aperture was 64 μm in diameter. The wavelength scale of the spectrometer was calibrated against Ho_2O_3 doped and Pr_2O_3/Nd_2O_3 doped standards (Hellma glass filters 666F1 and 666F7) with accuracy better than 15 cm^{-1} in the wavelength range 300-

1100 nm. Recorded spectra were fitted using the Jandel PeakFit 4.12 software assuming Gaussian peak shapes.

RESULTS AND DISCUSSION

The results of the chemical analyses (Table 2), which represent mean values of 6 spot analyses, were performed to obtain the average chemical compositions and estimates of compositional homogeneity. The studied crystal shows some chemical variations in terms of Mg, Mn and Zn. However, the Mn-content is substantial with a lowest concentration corresponding to ~5.2 wt% MnO. In addition, the analyses demonstrate that the transition element chemistry of the sample is quite simple comprising a major Mn component and very low concentrations of Fe (less than 0.43 wt% FeO). The spinel formula, calculated on the basis of 4 oxygen atoms, show that the present sample is dominated by Al (1.94 atoms per formula unit, apfu) and Zn (0.52 apfu) along with Mg (0.38 apfu). Hence, the studied spinel can be classified as Mg-rich gahnite ($ZnAl_2O_4$) containing significant amounts of both Mn^{2+} and Mn^{3+} (0.10 apfu and 0.06 apfu, respectively) as confirmed by optical absorption spectra (see below).

Site populations

The single-crystal-structure refinement results show that the m.a.n. at the tetrahedrally coordinated T site and octahedrally coordinated M site are 22.6 and 13.5, respectively. These values indicate that the T site is mainly occupied by Zn (Z = 30) and Mg (Z = 12) and the M site is not only occupied by Al (Z = 13) but also by heavier cations such as Mn (Z = 25). These site population is also supported by the values of T-O and M-O bond distances. In detail, the observed T-O =1.954 Å reflects a T site mainly occupied by Zn (expected value for ^{T}Zn-O equals 1.950 Å, where the M site is dominated by Al, Bosi et al. 2011) along with

significant amounts of ^{T}Mg [ideal bond distance 1.966(1) Å, Lavina et al. 2002]. The observed M-O = 1.921 Å reflects a M site dominated by Al [ideal distance 1.908(2) Å, Lavina et al. 2002] along with relatively minor amounts of larger cations such $^{M}Mn^{3+}$ [ideal distance 2.03(2) Å, Bosi et al. 2002; Lavina et al. 2002]. In order to translate the crystal chemical and structural refinement results into quantitative site populations at T and M, experimental and calculated data from the atom distribution were optimized. By using a least-squares program and the ideal bond distances of Lavina et al. (2002), except for ^{T}Zn-O (Bosi et al. 2011), the residuals between calculated and observed data (i.e., m.a.n. and bond distances) were minimized. Final residuals were within experimental uncertainties. The final structural formula for the present spinel is:

$$^{T}(Zn_{0.52}Mg_{0.34}Mn^{2+}_{0.08}Al_{0.06})_{\Sigma 1.00}\ ^{M}(Al_{1.88}Mn^{3+}_{0.06}Fe^{3+}_{0.01}Mg_{0.04}Mn^{2+}_{0.01})_{\Sigma 2.00}\,O_4$$

This formula is characterized by the almost complete dominance of divalent cations (i.e., Zn, Mg, Mn^{2+}) at the T site and trivalent cations (i.e., Al, Mn^{3+}) at the M site. A small degree of inversion (about 0.05), expressed as the fraction of divalent cations at M, also occurs.

Optical absorption spectrum

The recorded optical absorption spectrum (Fig. 1) shows a set of relatively narrow absorption bands centered at 26780, 25150, 23150, 21780 and 20300 cm^{-1}. In addition, there are two relatively broad absorption features centered at 23600 and 21200 cm^{-1}. All these bands are superimposed on a strong UV-edge absorption that rapidly falls off towards the visible spectral region and becomes insignificant in the green region of the visible spectrum.

At a first glance, the spectrum seems, with the exception of the strong UV-absorption edge to be almost identical to the spectrum of synthetic end-member galaxite, $MnAl_2O_4$, (Fig. 2) recorded by Hålenius et al. (2007, 2011). The strong UV-absorption edge in the present

spectrum is caused by O^{2-}-Mn^{3+} and O^{2-}-Fe^{3+} ligand-metal charge transfers (LMCT), which cannot occur in the spectra of the exclusively Mn^{2+}-bearing galaxite. Detailed inspection of the present spectrum discerns two additional major differences. Firstly, the narrow absorption bands occur at distinctly lower wavenumbers than the absorption bands in the spectrum of the end-member galaxite (Fig. 2). The absorption bands recorded in the galaxite spectrum (Hålenius et al. 2007; 2011), which are caused by spin-forbidden transitions in tetrahedrally coordinated Mn^{2+}, occur at 27780, 25970, 23390 [$^6A_1(S) \rightarrow {}^4Eg^4A_{1g}(G)$ transition], 22250, 20245 cm^{-1} (Hålenius et al. 2007, 2011). The corresponding absorption bands in the present Mn-bearing gahnite occur at energies that are up to 1000 cm^{-1} lower. Secondly, based on the concentration of tetrahedrally coordinated Mn^{2+}, the molar absorption coefficients (ε) of the bands in the present gahnite spectrum are in the range 3-25 L/mol·cm. This is one order of magnitude higher than the values of 0.1-1.9 L/mol·cm recorded for the absorption bands caused by spin-forbidden single ion transitions in tetrahedrally coordinated Mn^{2+} in spectra of the spinel (*sensu stricto*)-galaxite series (Hålenius et al. 2007, 2011).

The two broad bands observed in the present gahnite spectrum at 23600 and 21200 cm^{-1} occur at the energies recorded for spin-allowed *d-d* transitions in octahedrally coordinated Mn^{3+} in spectra of synthetic Mn^{3+}-bearing spinels (Bosi et al. 2007). The widths of these two bands are also comparable to those recorded in spectra of the synthetic samples. Based on the molar absorption coefficients of these two bands in spectra of the synthetic samples, the content of octahedrally coordinated Mn^{3+} in the present gahnite is calculated to be about 0.04 apfu. This value is consistent with the content of 0.056 (±0.020) apfu Mn^{3+} obtained from the electron microprobe analyses.

A third relatively strong and broad absorption band at 10800 cm^{-1} was recorded in the

spectrum of synthetic Mn^{3+}-bearing spinels and was assigned to a spin-allowed *d-d* transition in tetrahedrally coordinated Mn^{3+} (Bosi et al. 2007). This band is not observed in the present spectrum of a Mn-bearing gahnite (Fig. 1 and 2). Consequently, it is concluded that Mn^{3+} is ordered at the octahedrally coordinated site in the present sample.

The origin of the set of relatively narrow and intense absorption bands detailed earlier remains to be discussed. We can initially conclude that the present spinel contains four different transition element cations that may potentially give rise to narrow spectral bands through spin-forbidden electronic single ion transitions: $^{VI}Mn^{2+}$, $^{IV}Mn^{2+}$ and $^{VI}Mn^{3+}$, $^{VI}Fe^{3+}$. The last species can be excluded as the content of octahedrally coordinated ferric iron is simply too low to account for the intensity of the observed bands. Furthermore, the energies of the most intense spin-forbidden bands due to $^{VI}Fe^{3+}$ in spinel oxides are at 23000, 21600 [$^6A_1(S) \rightarrow {}^4E_g{}^4A_{1g}(G)$ transition] and 15050 cm^{-1} (Taran et al. 2005). We do not observe these bands in the present spectra. On the basis of band intensities and comparisons with spectra of synthetic Mn^{3+}-bearing spinel (Bosi et al. 2007), we can exclude spin-forbidden transitions in $^{VI}Mn^{3+}$ as the origin for these bands. We can also exclude single ion $^{VI}Mn^{2+}$ transitions on the basis of the comparatively low energy of the narrow absorption bands in the present spectrum. For instance, the characteristic, narrow and intense band due to the $^6A_1(S) \rightarrow {}^4E_g{}^4A_{1g}(G)$ transition in octahedrally coordinated Mn^{2+} occurs at distinctly higher energies (24000-25000 cm^{-1}) in spectra of oxygen-based minerals (Burns 1993 and references therein, Hålenius et al. 2007). As mentioned previously, the set of narrow absorption bands in the present spectrum shows a strong similarity with the absorption spectrum due to $^{IV}Mn^{2+}$ in spinels. However, the bands are displaced towards lower energies their intensities are an order of magnitude higher. We can therefore conclude that the recorded narrow absorption bands observed in the spectrum of the present Mn-bearing gahnite are not caused by any spin-forbidden single ion

transitions.

In parallel with the assignment of intensity enhanced narrow absorption bands in spectra of gahnite to electronic transitions in exchange coupled $^{VI}Fe^{3+}$- $^{IV}Fe^{2+}$ pairs (Taran et al. 2005), we must seek the origin of the observed narrow absorption bands (Fig. 1) in transitions taking place in manganese cation pairs. The chemistry and cation distribution of the present gahnite sample allow for a number of possible cation pair candidates: $^{VI}Mn^{2+}$- $^{VI}Mn^{2+}$, $^{IV}Mn^{2+}$- $^{VI}Mn^{2+}$, $^{IV}Mn^{2+}$- $^{IV}Mn^{2+}$, $^{VI}Mn^{2+}$- $^{VI}Mn^{3+}$and $^{IV}Mn^{2+}$- $^{VI}Mn^{3+}$. Most of these potential cation pairs can be excluded by comparisons with the recorded spectra of crystals belonging to the spinel (*sensu stricto*)-galaxite solid solution (Hålenius et al. 2011). The narrow absorption bands in the spectra of their synthetic samples showed constant molar absorption coefficients (ε) with respect to [$^{IV}Mn^{2+}$]-concentration and almost constant band energies within the entire solid solution series although pair concentrations of their samples increased with increasing total Mn-content (Hålenius et al. 2011). This suggests that the bands recorded in their spectra of spinel-galaxite crystals were caused by spin-forbidden electronic transitions in single-ion Mn^{2+} cations. No trivalent manganese was present in their synthetic samples that contained appreciable contents of divalent manganese at the octahedral M-site (up to 0.16 apfu) and the tetrahedral T-site (up to 0.84 apfu). Hence, their samples contained $^{VI}Mn^{2+}$- $^{VI}Mn^{2+}$, $^{IV}Mn^{2+}$- $^{VI}Mn^{2+}$and $^{IV}Mn^{2+}$- $^{IV}Mn^{2+}$ cation pairs at concentration levels considerable higher than those of the present gahnite sample ($^{IV}Mn^{2+}$ = 0.01 apfu and $^{IV}Mn^{2+}$= 0.08 apfu). Still, their spectra did not show any intense and narrow absorption bands at the band energies recorded in the present spectra. Consequently, the three pair configurations $^{VI}Mn^{2+}$- $^{VI}Mn^{2+}$, $^{IV}Mn^{2+}$- $^{VI}Mn^{2+}$and $^{IV}Mn^{2+}$- $^{IV}Mn^{2+}$ may be excluded as causes for the bands observed in the present spectrum. Of the two remaining pair configurations, $^{IV}Mn^{2+}$- $^{VI}Mn^{3+}$ is the more likely one as it necessitates smaller shifts in terms of energy and molar absorption coefficients with respect

to the corresponding formal single ion transitions in Mn^{2+}. For the proposed pair transition related to the formal single ion $^6A_1(S) \rightarrow {}^4E_g{}^4A_{1g}(G)$ transition in Mn^{2+}, the energy shift for the corresponding $^{IV}Mn^{2+}$- $^{VI}Mn^{3+}$ pair transition is -240 cm^{-1} [23390 cm^{-1} in the spectrum of end-member galaxite (Hålenius et al. 2011) compared to 23150 cm^{-1} in the present spectrum] and its molar absorption coefficient increases ~9 times [ε~1.90 L/mol·cm in end-member galaxite (Hålenius et al. 2007) compared to ε~17 L/mol·cm in the present sample]. As single ion $^{VI}Mn^{2+}$ bands occur at distinctly higher energies and display molar absorption coefficients approximately one order of magnitude smaller than single ion $^{IV}Mn^{2+}$ bands (Burns 1993 and references therein), the resulting band energy shifts and band intensity enhancements would be considerably larger for a $^{VI}Mn^{2+}$- $^{VI}Mn^{3+}$ pair transition assignment of the bands recorded in the present spectra. Based on published energy data for spin-forbidden single ion $^{VI}Mn^{2+}$ bands (Burns 1993; Hålenius et al. 2007) the band energy of the present $^6A_1(S) \rightarrow {}^4E_g{}^4A_{1g}(G)$ related transition is ~850 to ~1850 cm^{-1} lower. The energy shift of the $^6A_1(S) \rightarrow {}^4E_g{}^4A_{1g}(G)$ related transition in Mn^{2+}-Me^{n+} pairs is generally very small with respect to the energy of the corresponding transition in the unperturbed Mn^{2+} cation, although shifts of up to -300 cm^{-1} have been reported (Ferguson et al. 1966a). Consequently, we prefer the assignments of the observed absorption bands to electron transitions in $^{IV}Mn^{2+}$- $^{VI}Mn^{3+}$ pairs.

Implications

The present study of a Mn-bearing gahnite demonstrates that electronic transitions in exchange coupled pairs (ECP) of non-iron transition metal cations may have significant effects on the physical properties of minerals. We have based our interpretation on arguments related to energies and molar absorption coefficients (ε) of bands recorded in optical absorption spectra. However, a large set of additional spectroscopies, ideally carried out at different pressures and temperatures, and magnetic susceptibility measurements are available

for detection of exchange interactions in transition metal cation pairs. We believe that detailed examinations of Fe-free or Fe-poor minerals rich in other transition element cations using combinations of these methods will show that non-iron related IVCT and ECP transitions are much more common as the cause for mineral color than so far realized. In particular, spectra of close-packed mineral structures, as, e.g., oxide spinel minerals will most likely show a large range of ECP and IVCT transitions, as, e.g., the recently recorded Cu^{+}-Cu^{2+} IVCT in Cu-bearing spinels (Fregola et al. 2012).

ACKNOWLEDGEMENTS

We thank Kjell Gatedal for donating the spinel-bearing specimen from Kittelgruvan. Chemical analyses were carried out with the kind assistance of Marcello Serracino to whom we are grateful. We are thankful for detailed and helpful comments by the official reviewers George Rossman and Michail Taran. We appreciate the efficient handling of the manuscript by the associate editor Kristina Lilova.

REFERENCES CITED

Birkelbach, F., Flörke, U., Haupt, H.-J., Butzlaff, C, Trautwein, A.X., Wieghardt, K. and Chaudhuri, P. (1998) Competing exchange interactions and ground-state variability: Linear homo- and heterotrinuclear manganese(III/IV) complexes with tris(dimethylglyoximato)metalate(II) tetraanions as bridging ligands. *Inorganic Chemistry*, **37**, 2000-2008.

Bosi, F., Hålenius, U., Andreozzi, G., Skogby, H. and Lucchesi, S. (2007): Structural refinement of Mn-doped spinel: a case for tetrahedrally coordinated Mn^{3+} in an oxygen-based

structure. *American Mineralogist*, **92**, 27-33.

Bosi, F., Lucchesi, S., and Della Giusta, A. (2002) Structural relationships in $(Mn_{1-x}Zn_x)Mn_2O_4$ ($0 \leq x \leq 0.26$): The "dragging effect" of the tetrahedron on the octahedron. American Mineralogist, 87, 1121–1128.

Bosi, F., Hålenius, U., and Skogby, H. (2010) Crystal chemistry of the $MgAl_2O_4$-$MgMn_2O_4$-$MnMn_2O_4$ system: Analysis of structural distortion in spinel- and hausmannite-type structures. American Mineralogist, 95, 602–607.

Bosi, F., Andreozzi, G.B., Hålenius, U., and Skogby, H. (2011) Zn-O tetrahedral bond length variations in normal spinel oxides. American Mineralogist, 96, 594–598.

Burns, R.G. (1993) *Mineralogical Applications of Crystal Field Theory* (2nd edition), 551 p. Cambridge Univeristy Press, Cambridge, U.K.

Ferre, J. and Regis (1978) .*Solid State Communications*, **26**, 225-228.

Cador, O., Mathonière, C. and Kahn, O. (2000) Single crystal polarized optical absorption spectroscopy of the one-dimensional ferrimagnet $Mn^{II}Cu^{II}(pba)(H_2O)_3 \cdot 2H_2O$ (pba = 1,3-propylenebis(oxamato)). *Inorganic Chemistry,* **39**, 3799-3804.

Cox, N., Ames, W., Epel, B., Kulik, L.V., Rapatskiy, L., Neese, F., Messinger, J., Wieghardt, K. and Lubitz, W. (2011) Electronic structure of a weakly antiferromagnetically coupled MnIIMnIII model relevant to manganese proteins: A combined EPR, 55Mn-ENDOR, and DFT study. *Inorganic Chemistry*, **50**, 8238-8251.

Ferguson, J., Guggenheim, H.J., and Tanabe, Y. (1965a) Absorption of light by pairs of like and unlike transition-metal ions. *Physical Review Letters*, **14**, 737-738.

Ferguson, J., Guggenheim, H.J., and Tanabe, Y. (1965b) Exchange effects in electronic absorption spectrum of Mn(2) in perovskite fluorides. *Journal of Applied Physics*, **36**, 1046-1047.

Ferguson, J., Guggenheim, H.J., and Tanabe, Y. (1966a) Absorption of light by pairs of exchange-coupled manganese and nickel ions in cubic perovskite fluorides. *Journal of Chemical Physics*, **45**, 1134-1141.

Ferguson, J., Guggenheim, H.J., and Tanabe, Y. (1966b) The effects of exchange interactions in the spectra of octahedral manganese II compounds. *Journal of the Physical Society of Japan*, **21**, 692-704.

Ferre, J. and Régis, M (1978) Optical determination of the Cu-Mn – exchange interaction in $K_2Cu_{1-x}Mn_xF_4$. *Solid State Communications*, **26**, 225-228.

Franz, P., Ambrus, C., Hauser, A., Chernyshov, D., Hostettler,M., Hauser, J., L.,Keller,| Krämer, K., Stoeckli-Evans, H., Pattison, P., Bürgi, H.-B. and Decurtins, S. (2004) Crystalline, mixed-valence manganese analogue of Prussian Blue: Magnetic, spectroscopic, X-ray and neutron diffraction studies. *Journal of the American Chemical Society*, **126**, 16472-16477.

Fregola, R.A., Bosi, F., Skogby, H. and Hålenius, U. (2012) Cation oredring over short-range and long-range scales in the $MgAl_2O_4$-$CuAl_2O_4$ series. *American Mineralogist*, **97**, 1821-1827.

Hålenius, U. & Skogby, H. (1996) Crystal field spectra of trivalent manganese in synthetic and natural (Na^+-Mn^{3+})-substituted diopside. *European Journal of Mineralogy*, **8**, 1231-1240.

Hålenius, U. (2011) Absorption of light by exchange coupled pairs of tetrahedrally coordinated divalent manganese in the helvite-genthelvite solid solution. *Periodico di Mineralogia*, **80**, 105-111.

Hålenius, U., Bosi, F. and Skogby, H. (2007): Galaxite, $MnAl_2O_4$, a spectroscopic standard for tetrahedrally coordinated Mn^{2+} in oxygen-based mineral structures. *American Mineralogist* ***92****, 1225–1231*.

Hålenius, U., Bosi, F. and Skogby, H. (2011) A first record of strong structural relaxation of TO_4 tetrahedra in a spinel solid solution. *American Mineralogist,* ***96***, 617-622.

Lavina, B., Salviulo, G., and Della Giusta, A. (2002) Cation distribution and structure modeling of spinel solid solutions. Physics and Chemistry of Minerals, 29, 10–18.

Lohr, L.L. (1972) Spin-forbidden electronic excitations in transition metal complexes. *Coordination Chemistry Reviews*, **8**, 241-259.

Lohr, L.L. and McClure, D.S. (1968) Optical spectra of divalent manganese salts II. The

effect of interionic coupling on absorption strength. *Journal of Chemical Physics*, **49**, 3516–3521.

Mattson, S.M. and Rossman, G.R. (1987) Fe^{2+}-Fe^{3+} interactions in tourmaline. *Physics and Chemistry of Minerals*, **14**, 163-171.

Mattson, S.M. and Rossman, G.R. (1988) Fe^{2+}-Ti^{4+} charge-transfer in stoichiometric Fe^{2+}, Ti^{4+}-minerals. *Physics and Chemistry of Minerals*, **16**, 78-82.

McCarthy, P.J. and Güdel, H.U. (1988) Optical spectroscopy of exchange-coupled transition metal complexes. *Coordination Chemistry Review*, **88**, 69-131.

Pelletier, Y. and Reber, C. (1995) Single-crystal absorption spectroscopy of binuclear complexes of iron (III) and manganese (III) with the μ-oxo-bis(μ-acetato)dimetal core. *Canadian Journal of Chemistry*, **73**, 249-254.

Pouchou, J.L. and Pichoir, F. (1991) Quantitative analysis of homogeneous or stratified microvolumes applying the model "PAP." In K.F.J. Heinrich and D.E. Newbury, Eds., Electron Probe Quantification, p. 31–75. Plenum, New York.

Rossman, G.R. (1975) Spectroscopic and magnetic studies of ferric iron hydroxy sulphates: intensification of color in iron (III) clusters bridged by a single hydroxide ion. *American Mineralogist*, **60**, 698-704.

Rossman, G.R. (1976) Spectroscopic and magnetic studies of ferric iron hydroxy sulphates:

the series $Fe(OH)SO_4 \cdot nH_2O$ and the jarosites. *American Mineralogist*, **61**, 398-404.

Rossman, G.R. and Mattson, S.M. (1986) Yellow Mn-rich elbaite with Mn-Ti intervalence charge transfer. *American Mineralogist,* **71**, 599-602.

Smith, G., Hålenius, U., Annersten, H. & Ackermann, L. (1983) Optical and Mössbauer spectra of manganese-bearing phlogopites: Fe^{3+}-Mn^{2+} pair absorption as the origin of reverse pleochroism. *American Mineralogist*, **68**, 759-768.

Taran, M. N., & Koch-Müller, M. (2011). Optical absorption of electronic Fe–Ti charge-transfer transition in natural andalusite: the thermal stability of the charge-transfer band. *Physics and Chemistry of Minerals*, **38**, 215-222.

Taran, M.N., Koch-Müller, M. and Langer, K. (2005) Electronic absorption spectroscopy of natural (Fe^{2+}, Fe^{3+})-bearing spinels of spinel s.s.-hercynite and gahnite-hercynite solid solutions at different temperatures and high-pressures. *Physics and Chemistry of Minerals*, **32**, 175-188.

Xie, Q.-W., Chen, X., Hu, K.-Q., Wang, Y.-T., Cui, A.-L. and Kou, H.-Z. (2012) Mixed valence trinuclear manganese (II/III) complexes of flexible tetradenate N_2O_2 ligands: Ferromagnetic versus antiferromagnetic coupling. *Polyhedron*, **38**, 213-217.

452

453

454

455

456

457 TABLES

458

459 TABLE 1. Selected X-ray diffraction data of the Mn-bearing gahnite from Nordmark (Sweden)

460 TABLE 2. Electron microprobe analyses of Mn-bearing gahnite from Nordmark (Sweden)

461

462

463

464

465

466 FIGURE CAPTIONS

467

468 FIGURE 1. Optical absorption spectrum of Mn-bearing gahnite. The recorded spectrum is

469 shown by the black dotted line. Fitted UV-edge absorption, absorption bands and the total

470 fitted spectrum are shown by thin solid lines.

471

472 FIGURE 2. Optical absorption spectrum of Mn-bearing gahnite (black solid line) compared

473 with the spectrum of a synthetic end-member galaxite (dark grey solid line; from Hålenius et

474 al. 2007). The $^{IV}Mn^{2+}$ content in the galaxite sample is 0.84 apfu (Hålenius et al. 2011), but is

475 only 0.08 apfu in the present gahnite. Corresponding absorption bands in the two spectra are

476 connected by grey straight lines.

TABLE 1. Selected X-ray diffraction data for the Mn-bearing gahnite from Nordmark (Sweden)

Crystal size (mm)	0.20 × 0.20 × 0.22	Reciprocal range *hkl*	$-15 \le h \le 12$; $-10 \le k \le 14$; $-15 \le l \le 14$
a (Å)	8.1123(3)	Set of read reflections	1527
u	0.26404(4)	Unique reflections	120
T-O (Å)	1.9536(6)	Redundancy	11
M-O (Å)	1.9210(3)	Absorption correction method	SADABS
T-m.a.n.	22.57(8)	Refinement method	Full matrix least squares on F^2
M-m.a.n.	13.46(4)	EXTI	0.0024(2)
T-U^{11} (Å^2)	0.00452(7)	*R* int. (%)	0.51
M-U^{11} (Å^2)	0.00388(9)	*R*1 (%) all reflections	0.90
M-U^{12} (Å^2)	–0.00035(6)	*wR*2 (%)	1.79
O-U^{11} (Å^2)	0.00415(11)	Goof	1.123
O-U^{12} (Å^2)	–0.00030(9)	Diff. Peaks (±*e*/Å^3)	–0.20; 0.21

Notes: *a* = unit-cell parameter; *u* = oxygen fractional coordinate; T-O and M-O = tetrahedral and octahedral bond lengths, respectively; T- and M-m.a.n.. = T- and M-mean atomic number; U^{11} = atomic displacement parameter; $U^{11} = U^{22} = U^{33}$ and $U^{12} = U^{13} = U^{23}$ (= 0 for *T*-site due to symmetry reasons); EXTI = extinction parameter; *R* int. = merging residual value; *R*1 = discrepancy index, calculated from *F*-data; *wR*2 = weighted discrepancy index, calculated from F^2-data; GooF = goodness of fit; Diff. Peaks = maximum and minimum residual electron density. Radiation, Mo-*K*α = 0.71073 Å. Data collection temperature = 293 K. Total number of frames = 1539. Range for data collection 8° < 2θ < 86°. Origin fixed at $\bar{3}m$. Space group $Fd\bar{3}m$. *Z* = 8 formula units. Spinel structure has cations at Wyckoff positions 8*a* ≡ T (1/8, 1/8, 1/8) and 16*d* ≡ M (1/2, 1/2, 1/2), and oxygen anions at 32*e* (*u*, *u*, *u*).

TABLE 2. Electron microprobe analyses of Mn-bearing gahnite from Nordmark (Sweden)

	Mean of 6 spots	Standard deviation
Al_2O_3 wt%	58.42	0.35
MgO	9.10	0.77
*MnO	6.37	1.41
*FeO	0.32	0.07
ZnO	25.15	2.17
Total	99.37	
Cations per formula unit based on four oxygen atoms		
Al	1.937	0.032
Fe^{3+}	0.008	0.002
Mn^{3+}	0.056	0.020
Mg	0.382	0.030
Mn^{2+}	0.096	0.026
Zn	0.522	0.040
Total	3.000	
e^-_{EMPA} (epfu)	49.42	
e^-_{SREF}	49.49	

**Notes*: Fe^{3+} and Mn^{3+} calculated from stoichiometry. Standard deviation on cations calculated by error-propagation theory. e^-_{EMPA} and e^-_{SREF} = number of electrons per formula unit (epfu) derived from electron microprobe and structural refinement (respectively).

Figure 1

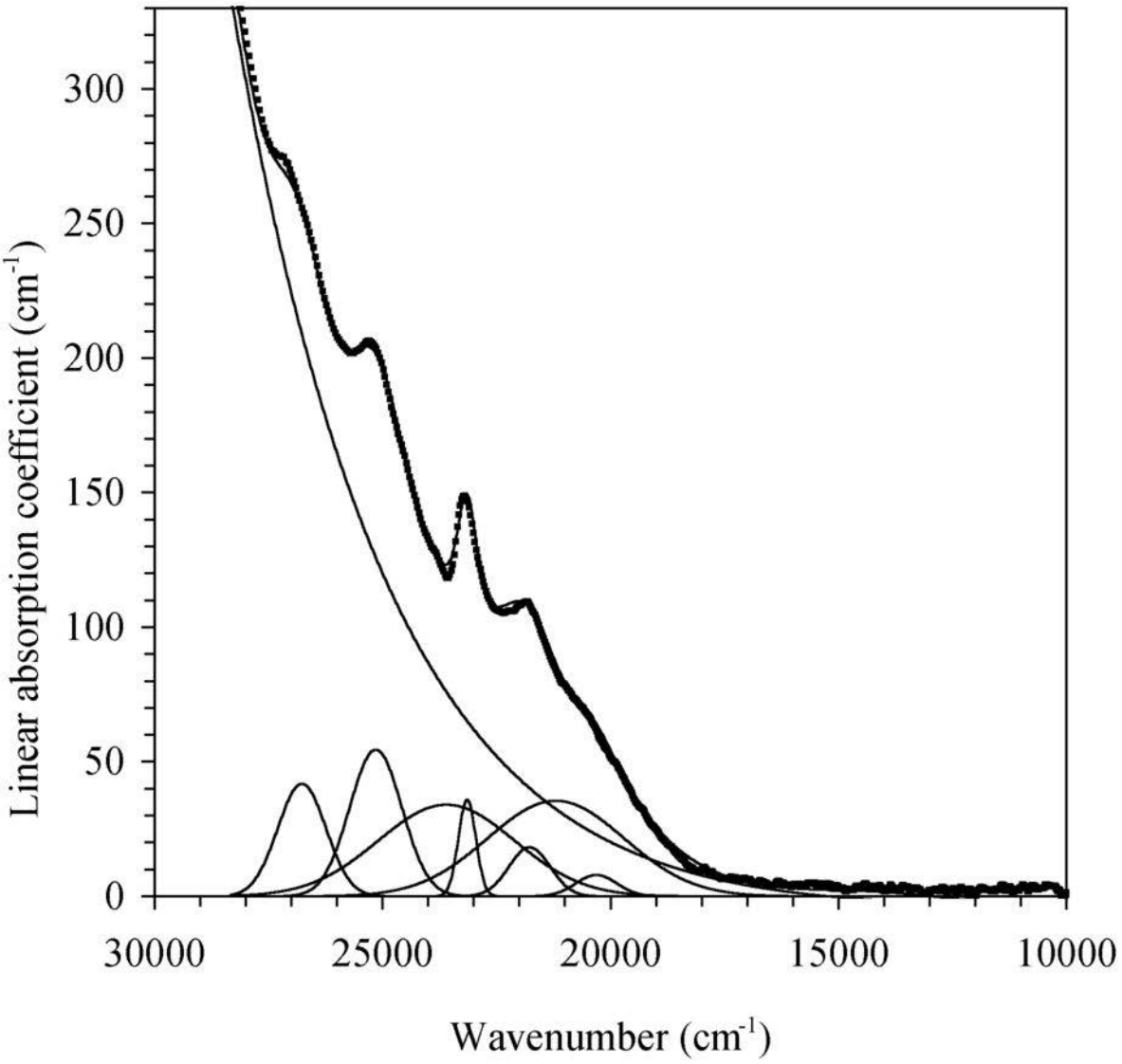
Linear absorption coefficient (cm-1)
300
250
200
150
100
50
0
30000
25000
20000
15000
10000
Wavenumber (cm-1)

Figure 2

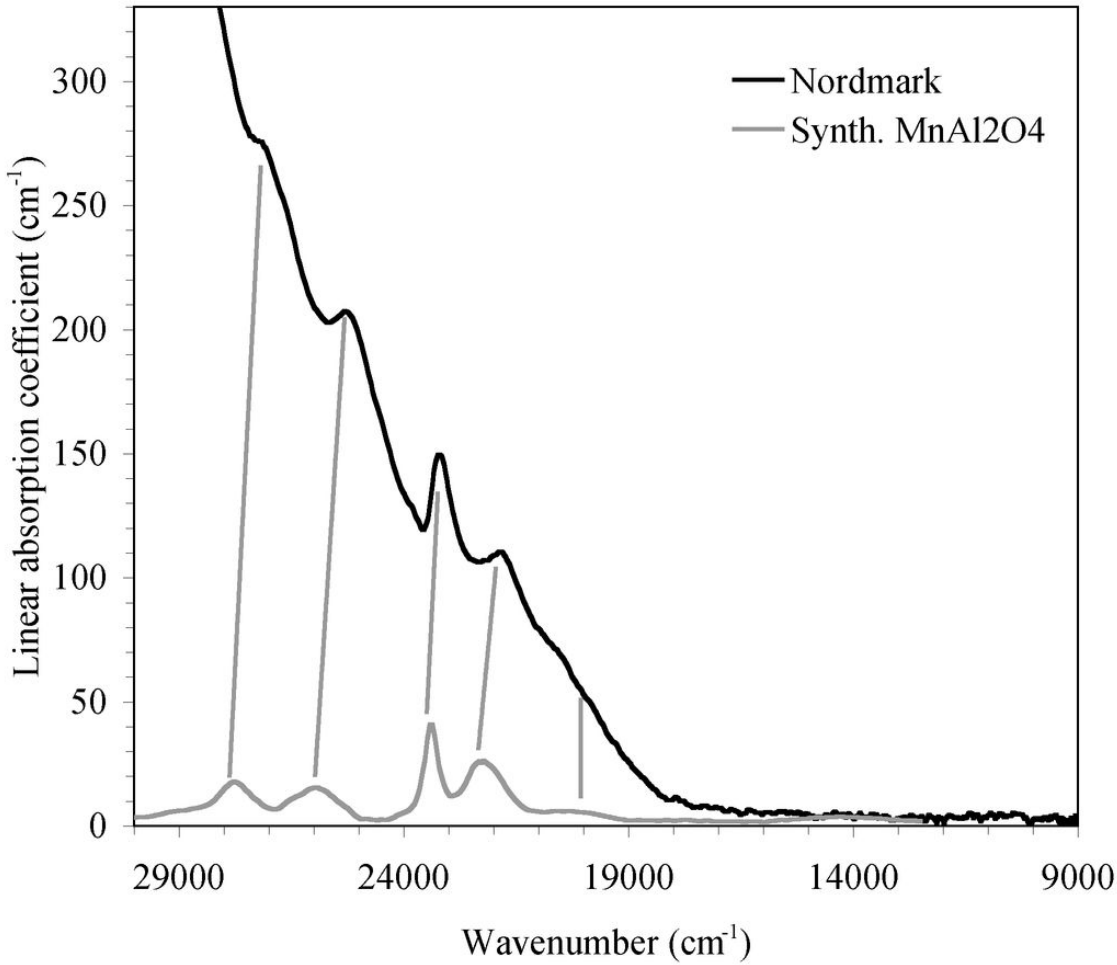
Nordmark
Synth. MnAl2O4
Linear absorption coefficient (cm-1)
300
250
200
150
100
50
0
29000
24000
19000
14000
9000
Wavenumber (cm-1)